PASSIVE DIRECTIONAL MOTION OF FLUID DURING BOILING DRIVEN BY SURFACE ASYMMETRY IN A DIELECTRIC FLUID

Sushil Bhavnani,^{1,*} Vinod Narayanan,² Naveenan Thiagarajan,³ & Logan Strid⁴

Original Manuscript Submitted: 8/1/2018; Final Draft Received: 1/13/2019

Passive thermal management is of interest in cooling of electronics and avionics in terrestrial and reduced gravity environments. This paper describes the use of microscale asymmetric surface patterns, or ratchets, to generate preferential fluid motion during phase change. The asymmetric patterns take the form of an array of ratchet structures. Preferentially directed bubble growth is demonstrated for boiling on surfaces with such ratchets augmented with re-entrant cavities to produce nucleation at preferred sites. During pool boiling in FC-72, the asymmetric geometry of microstructures causes bubbles to grow normal to the sloped surface rather than in a vertical direction, resulting in a net motion in a preferential direction. Bubble growth from the re-entrant cavities is studied using high-speed photography and image processing techniques. The concept of self-propulsion is extended to an open-ended channel configuration, wherein high-speed videos that document preferential motion of vapor slugs with velocities in the range of several mm/s are presented. Liquid motion is explained using a semi-empirical force balance.

KEY WORDS: phase change, microtextured surfaces, surface asymmetry, passive bubble-driven fluid motion

1. INTRODUCTION

Studies of bubble dynamics involved in liquid-vapor phase change and their interactions with the heated surface and the liquid are critical for understanding the underlying mechanism responsible for the enhanced heat transfer associated with boiling or phase change. Bubble dynamics, in general, over the past decades has been investigated for common fluids such as water or refrigerants such as R-113 and surfaces made of common metals. With the rising demands of high heat dissipation in modern high-power electronics, phase-change is well placed as an attractive

¹Department of Mechanical Engineering, Auburn University, Auburn, Alabama 36849, USA

²Department of Mechanical & Aerospace Engineering, University of California-Davis, Davis, California 95616, USA

³GE Global Research, Niskayuna, New York 12309, USA

⁴Space Exploration Technologies, Hawthorne, California 90250, USA

^{*}Address all correspondence to: Sushil Bhavnani, Department of Mechanical Engineering, Auburn University, Auburn, Alabama 36849, USA; Tel.: +1 334 844 3303; Fax: +1 334 844 3307, E-mail: bhavnsh@auburn.edu

NOMENCLATURE					
A_{inf}	area influenced by bubble	W	width		
	growth [Eq. (4)]	x	coordinate along ratchet surface		
A	curve-fit parameter for	y	coordinate perpendicular		
	inertia-controlled growth		to ratchet surface		
D	bubble diameter				
$egin{array}{c} F_s \ ec{F}_g \ f \end{array}$	shear force	Gree	k Symbols		
$ec{F}_g$	bubble growth force	α	ratchet angle (Fig. 13)		
f	bubble frequency	β	curve-fit parameter for heat		
h	height of liquid layer		transfer controlled growth		
L_1	length of long slope of ratchet	Δ	difference		
L_2	length of short slope of ratchet	μ	absolute viscosity		
L_3	ratchet pitch	ρ	density		
m	mass	σ	surface tension		
m	empirically derived	τ	shear stress		
	exponent [Eq. (2)]				
$ec{P_l}$	momentum imparted	Subs	ıbscripts		
P	pressure	1	location at crest of ratchet		
$q^{\prime\prime}$	heat flux	2	location at trough of ratchet		
r	radius of curvature	B	bottom wall of channel		
	of slug	d	departure		
t	elapsed time	g, v	vapor		
T	temperature	l	liquid		
u	liquid velocity in vicinity of slug	sub	subcooling		

cooling technique involving heat sink surfaces with microstructured silicon and dielectric fluids such as FC-72 (C_6F_{14}), a wetting fluid, which enable direct immersion cooling. These new combinations of surface structures and liquids alter the bubble dynamics significantly thereby generating the need for further studies.

T

w

top wall of channel

wall

liquid velocity in vicinity

of the bubble

 \vec{v}_l

Additionally, the ability to *passively transport* a heat transfer fluid is of great interest to several applications such as electronics and avionics cooling and spacecraft thermal management. This study presents a new phenomenon of self-propulsion of vapor slugs and liquid during nucleate boiling of fluid using asymmetry in surface structures. The asymmetry takes the form of a mm-sized ratchet array. An additional asymmetry in the form of preferentially located nucleation sites (cavities) is added to the ratchet. The impact of both asymmetries is assessed using two different experiments.

In the recent past, bubble dynamics have been manipulated for the development of bubblebased micropumps. Such micropumps are attractive for applications in electronics cooling since

the latent heat required for the bubble production is acquired from the heat that is to be dissipated from the microelectronic components, thereby leading to pump-less, power-free pumping with high heat dissipation. Phase-change-based micropumps, typically, use asymmetry to drive liquid through narrow- or micropassages. It has been demonstrated that periodic nucleation and collapse of vapor bubbles in a narrow cylindrical tube due to asymmetrically located heaters (Yuan and Prosperetti, 1999) can cause flow of liquid. Similarly, asymmetry in the form of location of heaters along a microchannel (Jun and Kim, 1998), which can be sequentially turned on to induce liquid pumping, was demonstrated. Powering the heaters sequentially, while turning the previous (upstream) heater off, caused a pressure gradient due to gradients in vapor pressure of the bubble and surface tension. This causes the bubble occupying the entire cross section to move towards the location of the heated area, thereby sweeping the liquid along. Linke et al. (2006) showed that in *film boiling*, an R-134a droplet on a heated surface in the form of asymmetric saw-tooth ratchets could be propelled at velocities up to 5 mm/s. The net viscous drag in the vapor layer between the liquid droplet and the ratcheted surface was hypothesized to be the driving force for the droplet motion. In a follow-up study, Ok et al. (2011) measured a maximum droplet velocity of 40 cm/s at a surface temperature of roughly 240°C with water using an 800 nm ratchet. While significant droplet velocities can be achieved in the Leidenfrost regime, the heat transfer rates are poor due to the presence of a vapor layer. Moreover, significantly high surface temperatures are needed relative to the fluid saturation temperature. However, for such micropumping systems to also be used as effective electronics cooling solutions, the systems need to operate in the nucleate boiling regime under a wide range of experimental conditions.

Similar to the test structure used in Linke et al. (2006), the study presented here discusses the development of a heat sink with a saw-tooth ratcheted cross-sectioned surface. Unlike the film-boiling regime tested in Linke et al. (2006), the study presented here discusses *nucleate boiling* of a dielectric liquid over the asymmetric silicon surface which is also enhanced with re-entrant cavities (vapor nucleation sites). The re-entrant cavities add to the asymmetry since they were fabricated only along the shallow slope of the ratchets, thereby promoting vapor nucleation along one side of the ratchets. During nucleate pool boiling, the shape of the structure and location of re-entrant cavities lead to an asymmetric nucleation, growth, and departure of vapor bubbles on the long slope as depicted in Fig. 1. It was shown by authors (Kapsenberg et al., 2012) in the past that such cyclic, asymmetric growth and departure of bubbles has the potential to produce a net lateral flow of liquid of up to 20 mm/s in water near the heated surface. A semi-empirical model based on momentum transferred due to the asymmetric growth was also presented.

Analytical bubble growth models developed in the past can broadly be classified into two types—bubble growth in uniform and non-uniform temperature fields. In the former, a vapor bubble grows in a uniformly superheated pool of liquid where the bubble growth is symmetrical. Models developed for the case of uniform temperature field can be divided into inertia-controlled growth (Rayleigh, 1917) and heat transfer controlled growth (Mikic et al., 1970; Plesset and Zwick, 1954; Scriven, 1959). These models have been subsequently extended for the case of bubble growth in a non-uniform temperature field like those of Zuber (1961), Cole and Shulman (1966), van Stralen (1975), and Mikic and Rohsenow (1969). These models do not necessarily extend to usage with structured surfaces and highly wetting fluids such as FC-72. Models for experimental conditions that are similar to those in the current study are mostly empirical in nature and often present asymptotic growth relationships as a function of time (Lee et al., 2003; Ramaswamy et al., 2002).

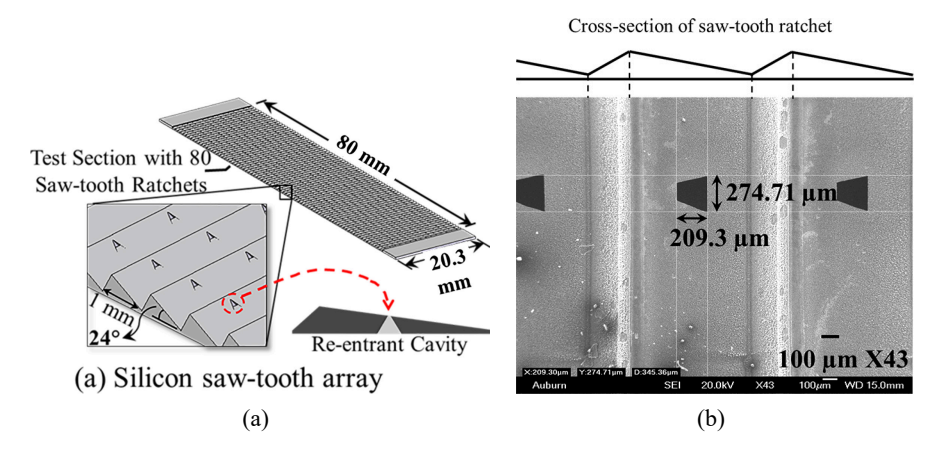


FIG. 1: (a) Test surface consisting of the asymmetric silicon ratchets with a footprint of 80 mm × 20.3 mm. (b) The re-entrant cavities are etched on the shallow slope of the ratchets as shown in the SEM image.

In this study, the growth of vapor bubbles in FC-72 nucleating from re-entrant cavities on a sloped silicon surface is experimentally characterized, contributing to an understanding of bubble growth on enhanced surfaces in dielectric fluids. Comparisons of the acquired information were made with the limited data available for conditions that are similar to those of the current study (Hutter et al., 2010; Demiray and Kim, 2004). The study and analysis of individual bubble dynamics is then extended to the flow of the two-phase mixture in an open-channel configuration to demonstrate the preferential directional motion. An open-channel configuration is defined as one in which the ends of the channel containing ratcheted walls are exposed to the same pressure.

2. EXPERIMENTAL SETUP

The experimental study was conducted in two stages. In the first stage, bubble dynamics from a flat ratcheted surface in a pool was studied to show nucleation and bubble growth in a preferred direction. In the second stage of experiments net fluid motion was studied in an open-channel configuration in the absence of preferentially located cavities.

2.1 Asymmetry due to Cavity Location

The intent of the pool-boiling experiment was to assess the impact of locating a cavity on one of the ratchet walls on the fluid. It was known from prior work by the group using water as the working fluid that a net lateral (parallel to the heater surface) motion of liquid surrounding the bubble can be attained in such a pool-boiling configuration. The present work advances the work by Kapsenberg et al. (2012) to a dielectric fluid and by characterizing bubble growth rates from such pyramidal re-entrant cavities in detail. The silicon test device used for the pool-boiling experiments shown in Fig. 1(a) comprises of two layers—the asymmetric ratcheted heat sink, and a serpentine aluminum heater. The heat sink has an asymmetric saw-tooth cross section with a 24°-90°-66° profile and 1 mm pitch. The angles are an artifact of the etching process described below and depend on etch selectivity. The heat sink constitutes 80 such ratchets spanning a footprint of 80 mm × 20.3 mm. The long shallow slope of each saw-toothed ratchet features reentrant cavities, or vapor trapping sites, that aid in triggering bubble nucleation. The re-entrant

cavities with a pyramidal cross section have a trapezoidal mouth of size ranging between 200 and 250 μm . A scanning electron microscope (SEM) image of the cavities is shown in Fig. 1(b). Each ratchet has eight cavities spaced equidistant along the ratchet on the shallow slope and in total the heat sink consists of 640 cavities acting as nucleation sites. Heat was provided using an aluminum serpentine heater fabricated on silicon using standard microfabrication procedures. The voltage leads on the heater also aid in surface temperature measurement.

The asymmetric cross section of the ratchet was obtained using a combination of gray-scale photolithography and deep reactive ion etching (DRIE) processes. Gray-scale photolithography enables deposition of photoresist with a gradient in height on a silicon surface as shown in Fig. 2(a). The DRIE process involves converting the angle in photoresist to a desired angle in silicon as shown in Fig. 2(b). The pyramidal re-entrant cavities were fabricated using an anisotropic wet etching process [Fig. 2(c)] and the fabricated heat sink was bonded to the aluminum heater wafer using fusion bonding in an oven at 1000°C [Fig. 2(d)]. Details of the fabrication of the asymmetric structure with re-entrant cavities and heater are in Thiagarajan et al. (2011, 2012).

The fabricated test section is soldered on to a printed circuit board for electrical connections and under-filled for structural integrity. The test board was suspended from the lid into a pool of FC-72 contained in an aluminum boiling chamber (Fig. 3) of dimensions 33 cm × 23 cm × 22 cm $(L \times W \times H)$. A thermistor and a pressure transducer were used to measure liquid temperature and absolute pressure, respectively. A reflux coil condenser open to the atmosphere helped maintain atmospheric pressure inside the boiling chamber and condense the vapor. Prior to experiments, the FC-72 was thoroughly degassed by boiling using the submerged cartridge heaters in the boiling chamber. The cartridge heaters with a proportional-integral-derivative (PID) controller were also used to achieve the required liquid subcooling. The boiling chamber was equipped with quartz windows for high-speed imaging. The imaging system consisted of a Phantom V310 high-speed camera fitted with an Infinity K2SC long working distance microscope lens and close-up objectives. Images were captured at 3200 fps with a resolution of 1280 × 800. A 250 W halogen lamp was used as a light source. The test section heater was powered by a 220 V DC power supply. Data including the supplied current, voltage measurements from the test section heater, thermistor, and pressure transducer, were recorded using an NI data acquisition system and LabVIEW. Wall temperature was calculated from the test section heater resistance measurements using a linear relationship that was previously obtained by calibration. Calibration of heater resistance was performed in a convection oven with a National Institute of Standards and Technology (NIST) calibrated thermistor as a standard, by varying the oven temperature

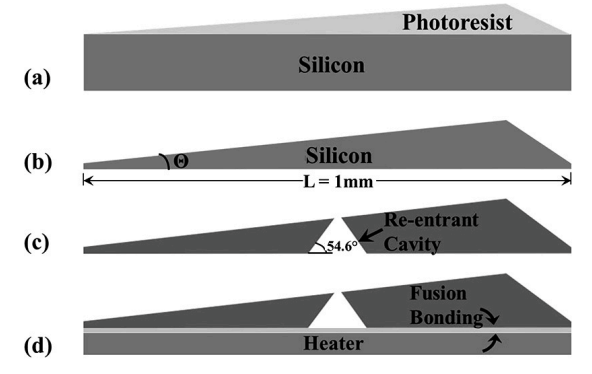


FIG. 2: Illustration of steps involved in test surface fabrication

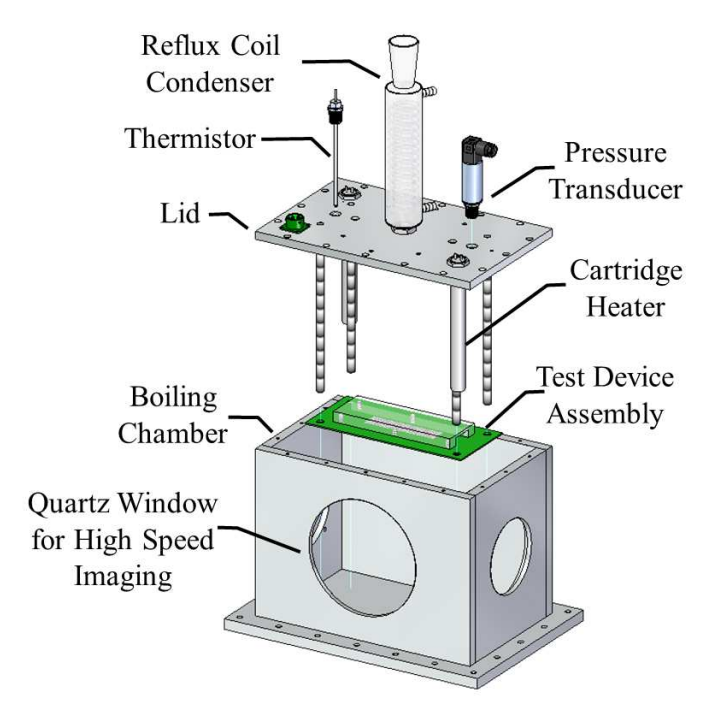


FIG. 3: Pool boiling chamber assembly

from 25°C to 85°C. Heat loss was quantified by attaching a thermocouple to the back of the test device. The uncertainty in measured wall temperature and heat flux is \pm 1% and \pm 0.3%, respectively.

2.2 Asymmetry due to Ratchet Angle

The intent of the open-channel configuration of experiments was to determine whether vapor slugs, formed by nucleating from walls with ratchets, would exhibit motion in a preferential direction due to the asymmetry of the ratchet geometry. A top view of the test chamber for the open-channel experiments is shown in Fig. 4. Both vertical walls shown comprised of 50 brass ratchets with a pitch of 1 mm [Fig. 4(b)], while the top and bottom walls are transparent to permit visualization. The brass ratchet walls did not contain any preferential cavities; the surface was uniformly sand-blasted with 80 micrometer particles. Because the surface area of the shallow slope was larger than that of the steeper slope, a large number of naturally occurring cavities were anticipated to exist on the shallow surface. Custom-fabricated serpentine thick film heaters, located on the backside of the brass ratchet walls, were used to supply heat. The backside of the heaters was insulated and the assembly consisting of the 76 mm long and 4.5 mm wide channel with heaters and insulation was located at the center of a 12.7 cm square × 1.27 cm high test chamber. A cooling coil was located at the periphery of this test chamber to condense the fluid and maintain the needed pool temperature. Video images were recorded at a location that is between the center and the exit of the open channel. The test chamber was placed on a laser table and leveled carefully to within + 0.2° from the horizontal. The video images were recorded at 500 frames per second.

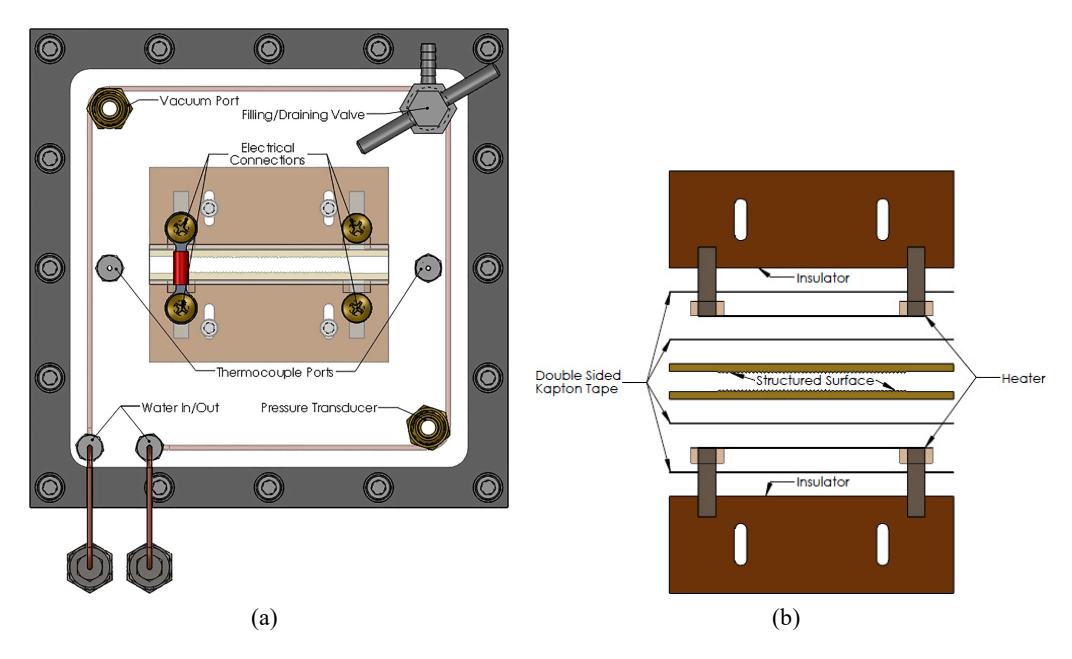


FIG. 4: Open-ended channel configuration (a) chamber as viewed from the top (b) top view detail of the heated vertical walls. The ratcheted surfaces comprise of the two vertical walls.

3. RESULTS

3.1 Asymmetry due to Cavity Location

Pool boiling experiments were conducted using FC-72 at atmospheric pressure. Bubble dynamics was studied using the high-speed images of bubble growth recorded during experiments. Figure 5 shows bubble departure from the re-entrant cavities on the shallow slope of the ratchets at a heat flux of 2.2 W/cm². It was observed that the bubbles grew and departed at an angle normal to the slope of the ratchets. The angle of departure could be noted by observing the angled line of departed bubbles in the saturated pool at the left end of the ratchet array. To further illustrate the bubble dynamics at the ratcheted surface, Fig. 6 shows a close-up image of bubble growth and departure from re-entrant cavities on the shallow slope of the ratchets. As discussed earlier, it can be observed that the bubble growth is normal to the slope of the ratchets and the bubbles depart in a direction normal to the sloped surface at high velocities. The vapor bubble eventually moves in a more vertical direction due to buoyancy effects after it has moved away from the immediate vicinity of the surface. The outline of several bubbles is enhanced using image processing for clarity. This asymmetric growth with respect to the vertical axis was consistent across the entire surface and at all tested heat flux and subcooling conditions.

Figure 7(a) shows one complete bubble ebullition cycle, consisting of bubble nucleation, growth, and departure from a re-entrant cavity at 1.6 W/cm² and saturated pool conditions. The vapor bubble nucleating from the cavity is initially hemispherical in shape. The hemispherical bubble grows rapidly mostly in a direction normal to the shallow slope of the ratcheted surface. This initial rapid bubble growth is inertia controlled where the driving potential for bubble growth is the temperature difference between the thin superheated liquid layer (relaxation microlayer) surrounding the bubble, and the vapor. During this initial rapid growth of the bubble

Havnani et al.

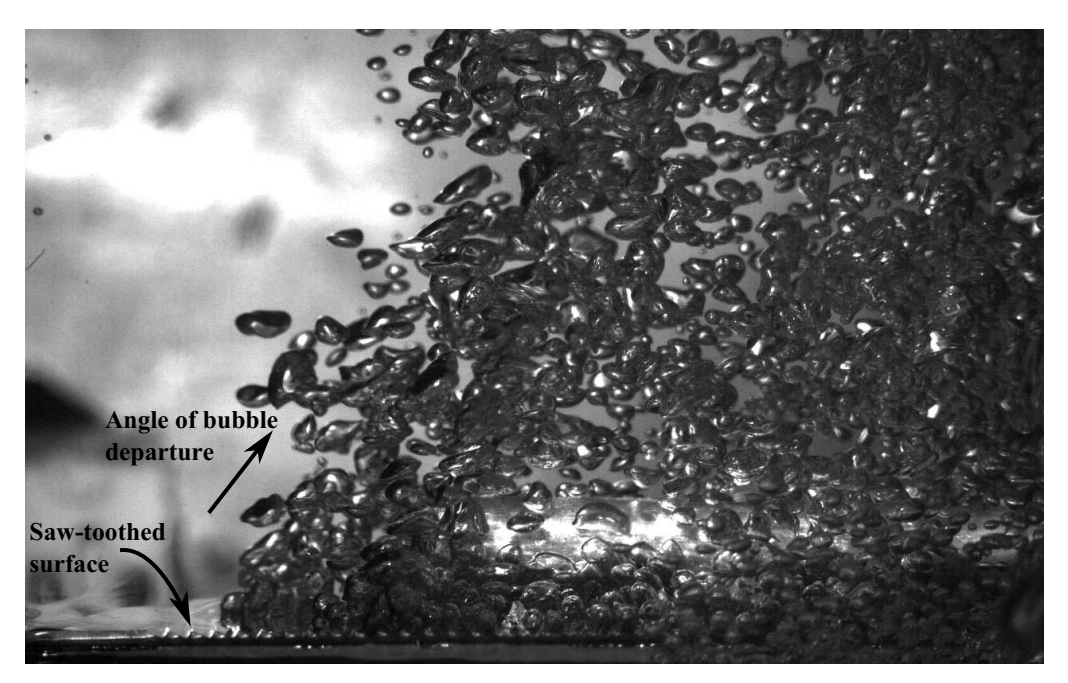


FIG. 5: Image showing bubble departure from re-entrant cavities at an angle normal to the sloped surface of the ratchets during saturated pool boiling at a heat flux of 2.2 W/cm².

normally into the pool, the bubble remains pinned to the cavity as the bubble footprint remains constant while the dome becomes more spherical. With increasing time, the dome grows larger in size, although at a considerably slower rate as the relaxation microlayer depletes. The growth continues until the buoyancy force is large enough to overcome the surface tension force that holds the bubble.

As the bubble begins to depart, the neck of the bubble narrows as it breaks and leads to bubble departure normal to the surface. It was also observed that the waiting time, the period between bubble departure and the initiation of nucleation of the next vapor bubble, was less than 312.5 µs, which was the time interval between two successive image frames.

An interesting observation from these bubble images was the shape of the bubble while it is attached to the surface. Vapor bubbles in highly wetting fluids such as FC-72 are generally observed to be more spherical and possess a very low contact angle due to the low surface tension of the liquid. However, in all the bubble images captured in this study the bubbles are consistently "light-bulb"—shaped and the contact angles appear to be very high, between 60° and 90°. Similar bubble shapes were also shown by Hutter et al. (2010) during pool boiling of FC-72 on a plain silicon surface with cylindrical cavities. This high contact angle also suggests that the evaporation microlayer, which often exists as a thin liquid layer underneath a bubble, is less significant or nearly absent. This can be largely attributed to the pinning of the bubble at the mouth of the cavity. It is the evaporation of this microlayer which has been shown in the past to contribute significantly to the rapid bubble growth in the inertia-controlled regime and high heat transfer rates involved in nucleate boiling (Cole and Shulman, 1966). However, Demiray and Kim (2004) studied the nucleate-boiling heat transfer under a single FC-72 bubble on a plain silicon surface and observed that the evaporation microlayer contribution is not significant

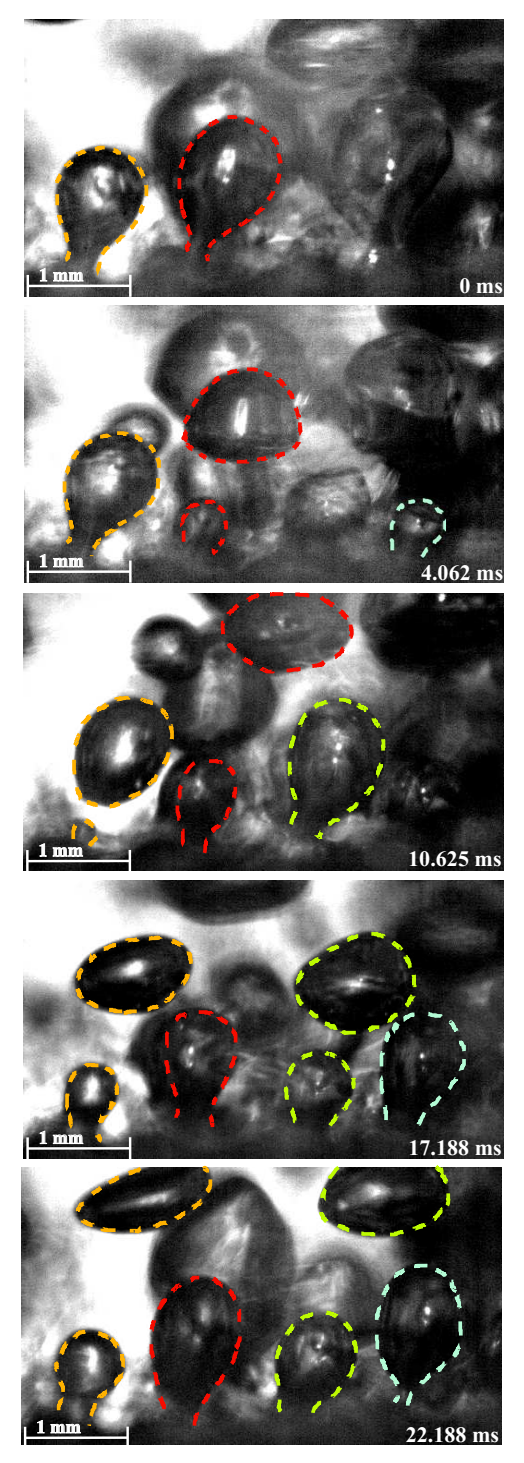


FIG. 6: Bubble growth and departure from re-entrant cavities at 2.2 W/cm² and saturated pool conditions. Bubbles nucleating from neighboring cavities are marked in different colors.

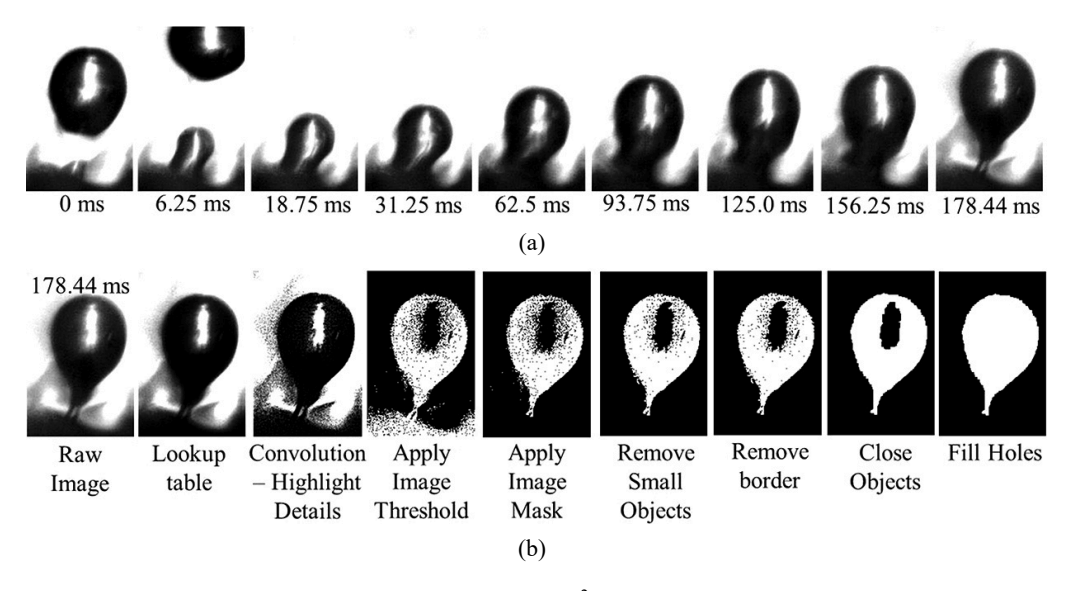


FIG. 7: (a) Ebullition cycle of a bubble at $q'' = 1.6 \text{ W/cm}^2$ and 21°C subcooling, and (b) image processing steps for the bubble frame at 178.44 µs in (a)

compared to transient conduction and microconvection contributions, which also supports the earlier observation about the absence of contribution from the evaporation microlayer in this study. Similar conclusions were also drawn by Hutter et al. (2010) in pool boiling of FC-72.

In the current study, bubble diameter was estimated from the captured images utilizing standard image processing techniques using NI Vision Assistant software. The series of steps involved in processing a single captured frame is shown in Fig. 7(b). The final image in the process is used to calculate projected bubble area and perimeter among other parameters. Using the projected area of the bubble from the final step of image processing shown in the figure, the diameter of the non-spherical bubble is calculated as the equivalent diameter of a projected circular disk with the same area as that of the bubble. This process is repeated for hundreds of frames involved in a single bubble growth cycle and multiple bubbles at different experimental conditions.

The bubble diameter estimated using this process during a single growth cycle is shown in Fig. 8. The growth of bubble involves a rapid initial inertia-controlled growth phase right after nucleation followed by a slower heat transfer controlled growth phase leading to departure. This observation agrees with the results reported in studies by Ramaswamy et al. (2002) and Hutter et al. (2010) for FC-72, and Lee et al. (2003) for R-11 and R-113. Using a linear curve fit for the inertia-controlled growth and a power-law fit for heat transfer controlled growth for the single bubble shown in Fig. 7, the asymptotic bubble growth rate relationship between bubble diameter and time can be obtained. For the inertia-controlled growth, the bubble diameter was observed to scale linearly with time, expressed as (following Rayleigh, 1917; and Mikic et al., 1970)

$$D = At (1)$$

where A is a curve-fit parameter that is a function of fluid properties and degree of superheat. This linear relationship is similar to the experimental growth rate reported in a number of other studies in the literature for the inertia-controlled regime. In the heat transfer controlled regime,

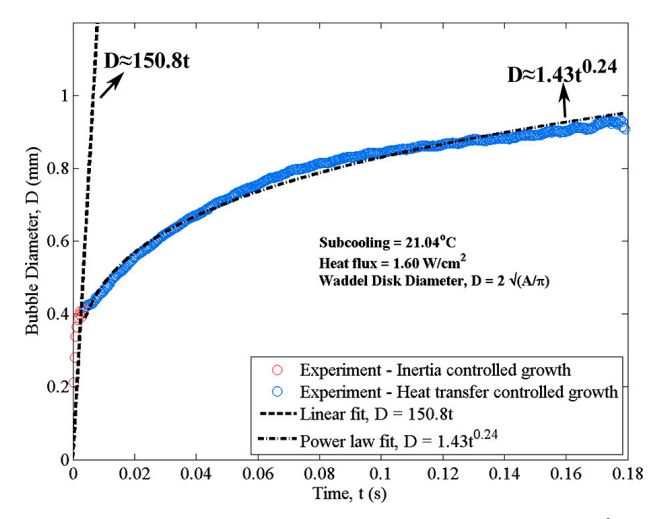


FIG. 8: Measured bubble growth for images shown in Fig. 7 at $q'' = 1.6 \text{ W/cm}^2$ and 21°C subcooling.

the asymptotic relationship is of the form

$$D \approx \beta t^m \tag{2}$$

where β and m are curve-fit parameters. The parameter β is a growth constant (following Scriven, 1959; Cole and Shulman, 1966) for the heat transfer controlled regime which is given as a function of wall superheat and flow properties.

The value of m for the experimental conditions shown in Fig. 8 is 0.24, which is much lower than the $t^{1/2}$ relationship reported by a large number of studies in the literature for water (Mikic et al., 1970; Cole and Shulman, 1966) and for FC-72 (Ramaswamy et al., 2002).

In a recent study conducted with FC-72 and structured cavities in silicon, Hutter et al. (2010) reported values of 0.37 and 0.53 for m, and in studies with saturated R-11 and R-113 Lee et al. (2003) observed m to be between $\approx 1/5$ and 1/3.

These bubble growth analyses were conducted at several heat flux values and several sub-cooling values. The data reinforce the primary concept indicating that bubble departure from a multitude of sites (640 on the surfaces studied) all nucleating from surfaces at the same inclination, acting in concert, have the ability to enable liquid motion in a preferred direction.

Figure 9 shows the effect of heat flux on bubble growth at a liquid subcooling of 21° C. As the heat flux increases, the wall superheat increases, leading to lower surface tension, causing an increase in bubble growth rate. These observations corresponding to the influence of heat flux, and hence wall temperature, on growth rate accord well with studies conducted especially with FC-72 such as Ramaswamy et al. (2002) and Hutter et al. (2010). In their studies, an increase in rate of bubble growth with increasing heat flux was also noticed in the inertia-controlled regime which is supported by the increasing value of A in the linear relationship, D = At. The experimental values of A for different heat flux values are summarized in Table 1. From Fig. 9, it can also be noticed that the transition from inertia- to heat-controlled regime occurs within a narrow range of bubble diameter, 0.45 to 0.55 mm, and is relatively insensitive to applied heat flux.

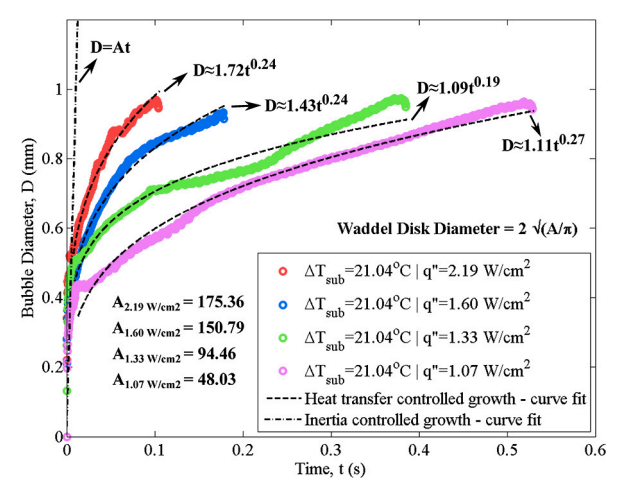


FIG. 9: Effect of heat flux on bubble growth at a liquid subcooling of 21°C

TABLE 1: Curve-fitting parameters from Fig. 9 for a subcooling of 21°C

Experimental	Bubble growth regime			
conditions	Inertia controlled	Heat transfer controlled		
Conditions	D=At (mm)	$D=eta t^m$ (mm)		
q'' (W/cm ²)	A (mm/s)	$\beta \text{ (mm/s}^m)$	m	
2.19	175.36	1.72	0.24	
1.60	150.79	1.43	0.24	
1.33	94.46	1.09	0.19	
1.06	48.03	1.11	0.27	

The bubble growth curve-fit expressions can be used in the bubble growth model of Kapsenberg et al. (2012) to arrive at an expression for liquid velocity surrounding the bubble and hence provide an estimate for the net horizontal (lateral) component of velocity imparted due to the bubble growth on the ratchet face. The model is based on the premise that the time rate of change of momentum imparted to the liquid surrounding the bubble should be provided by the growth of the bubble,

$$\frac{d\vec{P}_l}{dt} = \frac{d\left(m_l \vec{v_l}\right)}{dt} = \left|\vec{F}_g\right| \tag{3}$$

The mass of liquid displaced by the bubble is given by the area of liquid influenced by bubble growth, A_{inf} , density of liquid, the bubble departure frequency, and liquid velocity,

$$m_l = \rho_l A_{inf} |\vec{v}_l| f_d^{-1} \tag{4}$$

The growth force is modeled simply based on the drag force of the bubble moving at the bubble diameter growth rate,

$$\left| \vec{F}_g \right| = \frac{1}{2} \cdot \left(\frac{\pi D^2}{4} \right) \cdot \rho_l \cdot \left(\frac{\partial D}{\partial t} \right)^2 \tag{5}$$

Combining Eqs. (3)–(5), one can arrive at an expression for liquid velocity around the bubble in terms of the bubble growth rate and bubble departure frequency. The net lateral component of velocity can further be obtained as the cosine ratchet angle component of the determined velocity from the model. Kapsenberg et al. (2012) used high-speed imaging videos and determined a net liquid velocity by discretizing Eq. (5). With the bubble departure curve fits in this paper, a better estimate of the liquid velocity can be obtained. Based on the growth rates, it is anticipated that most of the liquid momentum would be imparted in the inertial-controlled growth regime. In order to develop a generalized model, further work is needed in incorporating models for bubble departure frequency and in relating the empirically fitted bubble departure diameters in this study into coefficients and exponents that include fluid subcooling and fluid properties in Eq. (1).

3.2 Asymmetry due to Ratchet Angle

High-speed videos were recorded at heat fluxes ranging from 0.35 to 5.22 W/cm², over a range of subcooling from 6.3°C to 55°C. Over the range of experimental conditions, mean bubble/slug velocities ranging from 13 to 95 mm/s were observed. Images were recorded at a location that is between the center and the exit of the open channel.

Three distinct regimes of self-propulsion were observed for the range of studied experimental conditions, namely the bubble regime, churn flow regime, and the intermittent slug regime. In the context of this work, bubbles refer to vapor masses that are typically less than or of the same scale as the width of the channel, while slugs refer to longer vapor masses that span a large extent of the channel. Churn flow denotes a regime wherein chaotic bubble formation and merger are noted. The bubble regime was observed under low heat fluxes (< 1.5 W/cm²) and high subcooling in excess of 20°C. Intermittent slug flow was observed at heat fluxes under 1.5 W/cm² and at subcooling between 5 and 25°C. Churn flow regime was observed at the higher heat flux of 2.7 W/cm² and a subcooling of 22°C. The direction of slug propulsion was along the long slope of the ratchets in these regimes. To ensure that the motion was not caused due to a slight tilt of the test chamber, the orientation of the test chamber was changed by 180° about a vertical axis, and some experiments were performed again. The direction of bubble motion was once again confirmed to be along the shallow slope of the ratchet.

The bubble regime is depicted in the series of images in Fig. 10. This regime occurred at a high subcooling and moderate to high heat fluxes ($\sim 5 \text{ W/cm}^2$ and 43.3°C) or at moderate heat

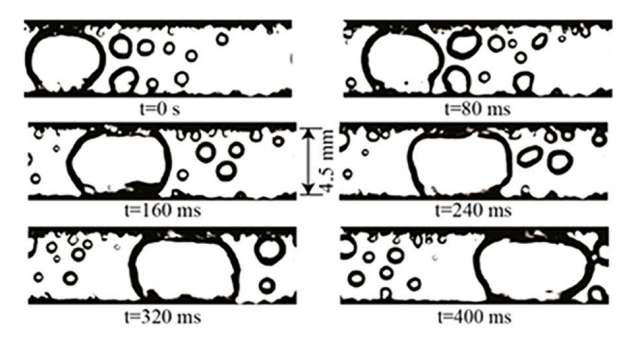


FIG. 10: Images captured from high-speed video show a large vapor bubble moving from left to right in an open channel and growing in size due to mergers with smaller bubbles. Both vertical walls seen in the images are comprised of 50 ratchets with a pitch of one mm, while the top and bottom walls are transparent to permit visualization.

fluxes to low heat fluxes (< 1.4 W/cm²) and moderate subcooling (21–28°C). In Fig. 10, the heat flux to the ratchet walls was 5.22 W/cm² based on the projected area and the fluid in the pool surrounding the open channel was maintained at 43°C subcooling. Small bubbles emanating from the structured surface occupied the channel and coalesced when in close proximity to another small bubble. These intermediate-size bubbles appeared to bounce or roll along the wall as they continued to collect smaller bubbles and grow until spanning the width of the channel. When sufficient departed bubbles merge to form a larger slug, the slug is propelled along the channel in a preferential direction, along the long (30°) slope of the ratchets. The large bubbles traveled at average velocities in the field of view ranging from 21 to 32 mm/s, and continued to gain size by coalescence with smaller bubbles, but never grew larger than the field of view.

Figure 11 shows the data of position and velocity with time of the center of mass of the slug in Fig. 10. Also presented are acceleration data for several consecutive slugs recorded in the same video sequence. Acceleration data are provided as a function of time to indicate the frequency of slug passage through the field of view. Position data were typically represented by a second-order curve fit with time, and velocities were linearly increasing with time while accelerations were positive. The average velocity of the center of mass of 6 slugs was 28.1 mm/s (\pm 2.3 mm/s) and the average acceleration was 44 mm/s² (\pm 18 mm/s²) over 6 consecutive slugs. Variations in velocity and acceleration between the slugs are attributed to differences in initial mass of the slugs in the field of view and mergers with smaller bubbles within the field of view.

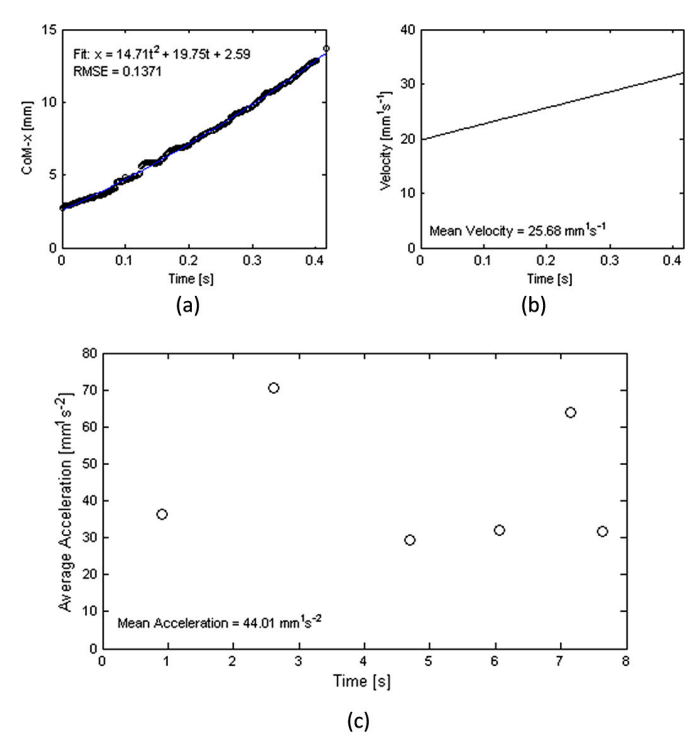


FIG. 11: (a) Position and (b) velocity of the center of mass (CoM) of the slug shown in Fig. 10 as a function of elapsed time. The acceleration of six such sequential slugs is shown in (c). Note that the velocity was determined from a best fit curve of position data to reduce noise due to unsteadiness caused by bubble mergers.

The churn flow (the first four images in Fig. 12) regime was characterized by the presence of large unstable bubble slugs with unstable and irregular interfaces. These slugs traveled rapidly through the channel at average velocities in the field of view ranging from 48 to 95 mm/s. This regime was observed in testing conditions with moderate to high heat flux ($> 2.0 \text{ W/cm}^2$), moderate subcooling (15–30°C), and a channel width of 4.5 mm.

The third regime was that of intermittent slugs (next four images in Fig. 12), wherein an initial bubbly flow was seen to coalesce to form large bubbles which span the width of the channel. Once a large bubble interface reached the structured surfaces on either side of the channel, it began to move down the channel, progressively merging with the other large bubbles to form a slug. The average velocity of slugs ranged from 24 to 71 mm/s in the field of view. The cycle repeated after the slug passed from the field of view. Intermittent slug flow regime was observed under one of the following conditions—low heat flux (0.6 W/cm^2) and low subcooling (6°C) or under larger heat fluxes $(\sim 1.7 \text{ W/cm}^2)$ and moderate subcooling $(\sim 17-26^{\circ}\text{C})$.

3.3 Slug Transport Model

The physical phenomenon of rapid transport of vapor slugs along the structured surface is not fully understood. Several mechanisms contribute to the motion of vapor within the channel depending on the heat flux and subcooling. For example, in the bubble regime, lateral motion of the fluid could be generated owing to the growth of individual bubbles on the face of the ratchet,

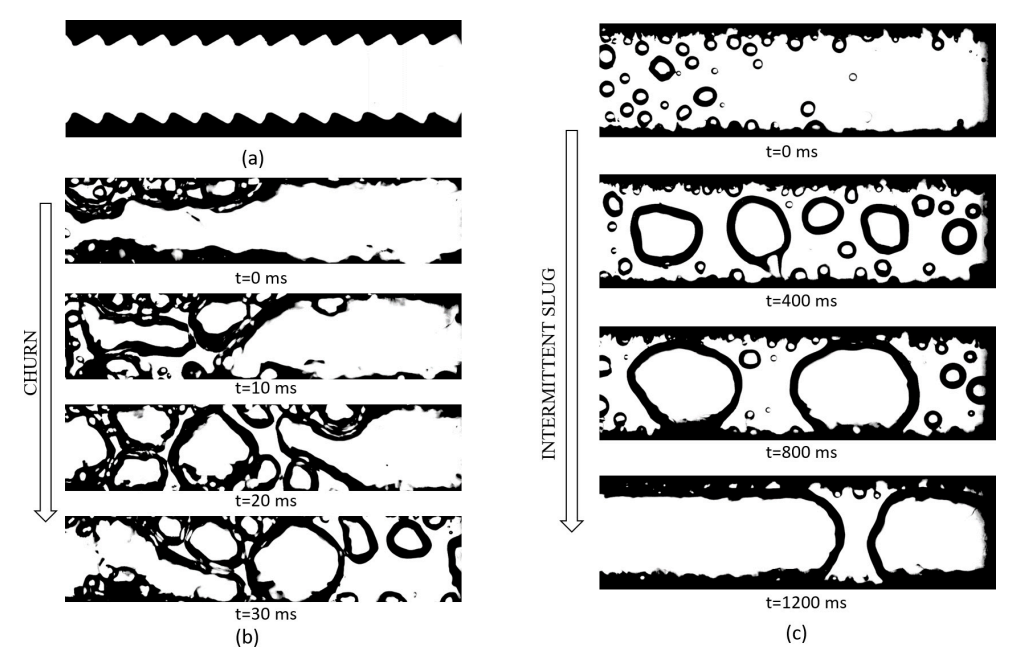


FIG. 12: Flow regimes observed under varying heat flux and subcooling conditions. (a) Reference image recorded in the absence of heating, (b) Sequence of four non-consecutive frames illustrating churn-like flow. $P=1.01\pm0.06$ bar, $\Delta T_{sub}=22.1\pm0.14$ °C, $q''=2.74\pm0.06$ W/cm², W=4.5 mm. Video capture details: 500 fps, Exposure Time = 90 μ s, Aperture 100% open. (c) Sequence of four non-consecutive frames illustrating intermittent slug flow. $P=1.01\pm0.06$ bar, $\Delta T_{sub}=17.7\pm0.14$ °C, $q''=1.37\pm0.04$ W/cm², w=4.5 mm. Video capture details: 500 fps, Exposure Time = 90 μ s, Aperture 100% open.

as discussed in Section 3.1. It was of interest to determine whether additional mechanisms due to the geometrical asymmetry of the ratchet could result in a net motion of a large growing vapor slug. In this section, a preliminary model to predict the net motion in slugs is presented. It is proposed that the asymmetric shape of the structured surface topography creates a pressure difference in the liquid over each ratchet and is the basis for driving flow. Such a driving force would be similar to that proposed by Linke et al. (2006) for the Leidenfrost droplet propulsion.

In order to verify slug transport in the absence of other mechanisms, a flash (homogeneous nucleation) experiment was performed. Such an experiment would preclude the possibility of bubble growth on the wall of the ratchet as a contributing mechanism to fluid motion. In the flash experiment, the pressure of the chamber was lowered such that the fluid temperature dropped below the saturation temperature at the corresponding pressure and the ratchet walls were unheated. The experimental chamber was connected to a vacuum tank and the pressure was reduced until phase change was observed. Figure 13 shows a video sequence of the observed large slugs, indicating the same directional motion as observed in the diabatic test (Figs. 10 and 12). The chamber pressure was maintained at 0.29 bar and the pool and saturation temperature was 24.5°C (zero subcooling). The ratchets are clearly visible in these images as compared with the earlier images, due to the absence of density gradients caused by heating of the walls.

Velocity and acceleration of the leading edge of the slugs were determined upon image processing. Average velocities in the field of view of the leading edge were seen to vary over a narrow range of 55 to 65 mm/s with a positive average acceleration of 152 mm/s². Images in Fig. 13 suggest that the slug is in contact with the ratcheted surface on either side of the channel; however, there exists a thin liquid layer that separates the bubble from the solid surface. Liquid layer thickness was measured for a series of frames using National Instruments Vision Assistant software. One clearly viewable ratchet was selected as the region of interest for the analysis. An *in situ* frame showing this ratchet with no slug present was chosen for analysis and the location and geometry of the ratchet was determined with edge detection as indicated in Fig. 14(a). Next, the radii of curvature of the slug at the crest (r_1) and troughs on the steep and shallow faces (r_2) were determined using circular edge detection [Fig. 14(b)]. A series of forty-two consecutive

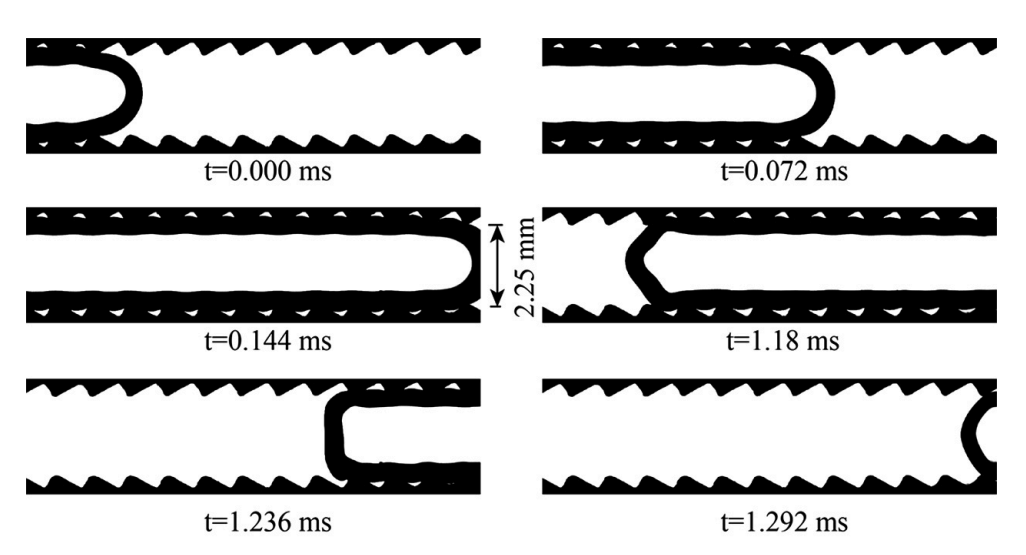


FIG. 13: Video sequence recorded during a flash test. The ratchets are unheated.

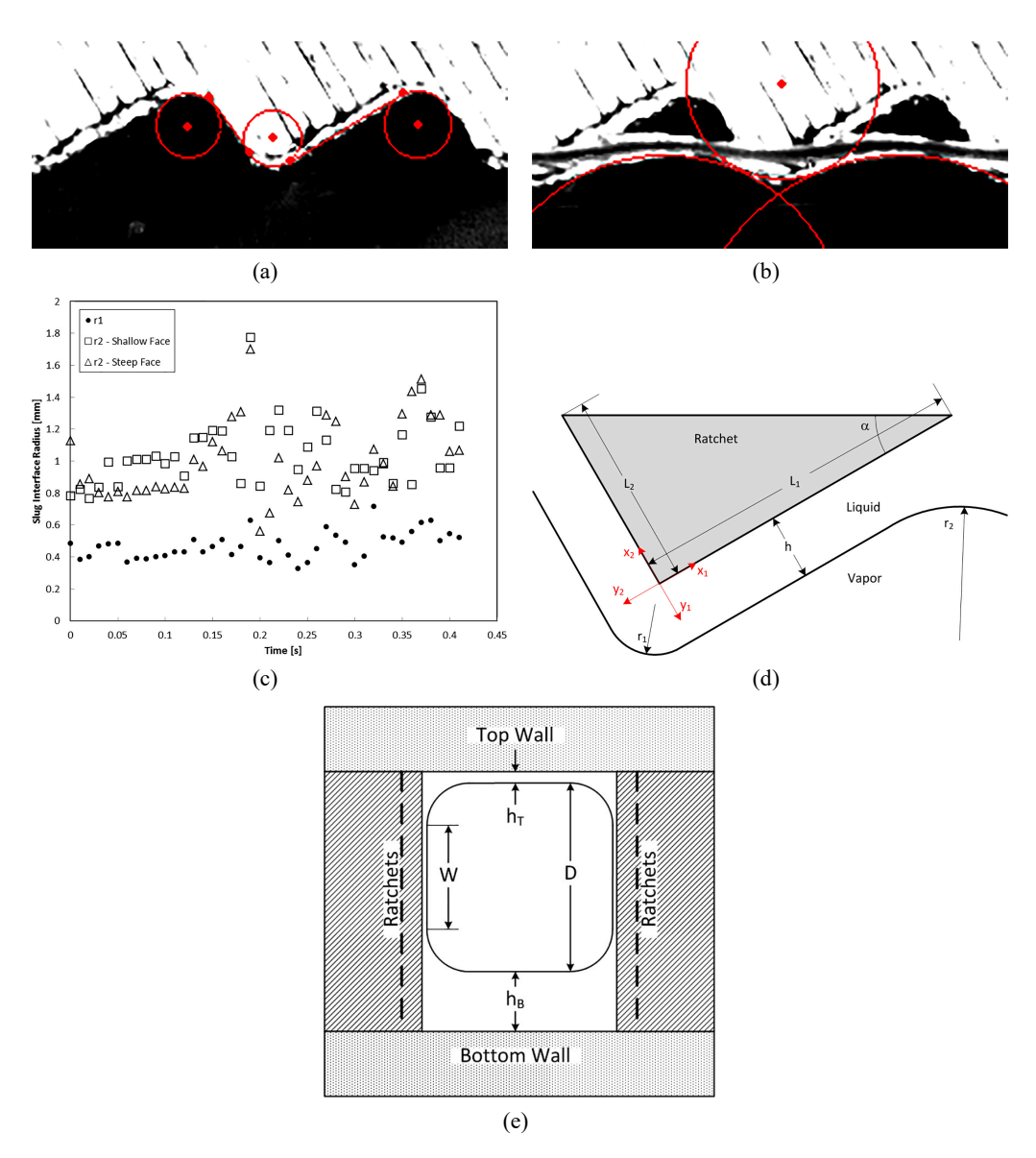


FIG. 14: Determination of the liquid layer thickness, h, and radii of curvature, r, for the Couette–Poiseuille flow model. Edge detection applied to (a) the base ratchets, and (b) to the vapor slug. The variation of the magnitude of radii of curvature of the slug over 42 consecutive frames is shown in (c) indicating the difference in the radii of curvature at the trough and peak. A simplified schematic of the liquid layer between the ratchet and the slug is shown in (d) identifying the parameters of importance in the model. A cross-sectional schematic of the bubble is shown in (e) indicating the hypothesized bubble shape and corresponding liquid layer thicknesses between the slug and the top and bottom walls.

frames were analyzed similarly to determine the radii of the bubble interface near the solid surface, as shown in Fig. 14(c). As seen in Fig. 14(c), the radii at the trough, r_2 on the shallow, and steep faces were nearly identical and are assumed equal.

Figure 14(d) represents a simplified schematic of the liquid layer in between the ratchet wall and the vapor slug. It is seen that r_1 is concave, indicating that the vapor pressure within the bubble at the peak, $P_{1,v}$, is lower than the local liquid pressure, $P_{1,l}$. Conversely, the radius of curvature of the slug at the trough, r_2 , is convex; the vapor pressure within the bubble at the trough, $P_{2,v}$, is greater than the local liquid pressure, $P_{2,l}$. The pressure difference between the vapor and liquid at each location is determined using the Young–Laplace equation.

Assuming that the vapor pressure is equal throughout the bubble (i.e., $P_{1v} = P_{2v}$), a pressure difference in the liquid layer between the peak and trough exists and is given as

$$P_{1,l} - P_{2,l} = \sigma \left(\frac{1}{r_1} - \frac{1}{r_2} \right) \tag{6}$$

where locations 1 and 2 correspond to the crest and trough of the ratchet, and r corresponds to the radius of the slug, respectively.

This pressure difference exists along the long slope (L_1) as well as the short slope (L_2) of the ratchet. However, due to the asymmetry in L_1 and L_2 as well as their subtended angle to the horizontal, a net driving pressure gradient exists along the long slope of the ratchet. The velocity of liquid in this layer is determined by a balance between this net driving pressure differential and the retarding viscous shear force. Assuming an average height, $h[h=(h_1+h_2)/2=211\,\mu\text{m}]$ of the liquid layer and using a Couette-Poiseuille flow model, the velocity of the liquid along direction x_1 [see Fig. 14(d)] can be given as

$$u(x_1) = -\frac{1}{2\mu} \frac{dP}{dx_1} \left(hy - y^2 \right) + \frac{V}{h} y \tag{7}$$

where V is the velocity of the vapor slug and dP/dx_1 can be related to the surface tension and radii of curvature from Eq. (6). The shear stress can be determined from Eq. (7) as

$$\tau_w = -\tau_{yx}|_{y=h} = -\mu \left. \frac{du}{dy} \right|_{y=h} = -\frac{h}{2} \frac{\partial P}{\partial x_1} - \frac{\mu V}{h} \tag{8}$$

where μ is the fluid dynamic viscosity, and h is the average liquid layer thicknesss between the slug and the ratchet wall. Integrating the shear stress acting on the slug along the length of the ratchet face provides the total shear force per unit width,

$$\frac{F}{W} = -\int_0^{L_1} \tau_w dx = \left[\frac{\mu V}{h} + \frac{h}{2} \frac{\partial P}{\partial x_1} \right] L_1 \tag{9}$$

where L_1 is the length along the shallow face of the ratchet, and W is the width of the bubble interacting with the ratchet [Fig. 14(e)].

The component of this force acting in the direction of travel of the bubble (horizontal) is therefore

$$F_{\Delta P1} = \left[\frac{\mu V}{h} + \frac{h}{2} \frac{\partial P}{\partial x_1}\right] L_1 W \cos \alpha \tag{10}$$

where α is 30° and L_1 is 0.880 μ m for the ratchet pitch of 1000 μ m. Applying the same analysis to the steep slope of the ratchet using x_2 , y_2 , and L_2 , with the same liquid layer thickness an opposing force to the flow is found. The net driving force per ratchet acting on the slug in the direction of x_1 is

$$F_{\Delta P} = \left[\frac{\mu V}{h} + \frac{h}{2} \frac{\partial P}{\partial x_1}\right] L_1 W \cos \alpha - \left[\frac{\mu V}{h} + \frac{h}{2} \frac{\partial P}{\partial x_2}\right] L_2 W \sin \alpha \tag{11}$$

where L_2 is the length along the steep slope of the ratchet [Fig. 14(d)]. In the backlit imaging shown in Fig. 13, a thick boundary can be seen at the interface of the bubble. Due to the short depth of field (80 μ m) of the lens used, this dark region corresponds to the curvature of the bubble; thus, the width W_T in Fig. 14(e) corresponds to a flat liquid film in contact with the top wall of the channel. The flat region width is measured via image processing. Assuming that the slug is symmetrical for the case of homogeneous nucleation, the width W is estimated to be identical to W_T .

The retarding force is in the form of shear imparted by the top and bottom walls,

$$F_S = \mu V \left[\frac{1}{h_T} + \frac{1}{h_B} \right] L_3 W \tag{12}$$

where L_3 is the pitch of the ratchet,

$$L_3 = L_1 \cos \alpha + L_2 \sin \alpha \tag{13}$$

and h_B can be estimated from Fig. 14(e) to be based on the channel height and bubble depth, D. Combining the driving and retarding forces, an expression can be obtained for equilibrium velocity of the slug,

$$2\left\{ \left[\frac{\mu V}{h} + \frac{h}{2} \frac{\partial P}{\partial x_1} \right] L_1 \cos \alpha - \left[\frac{\mu V}{h} + \frac{h}{2} \frac{\partial P}{\partial x_2} \right] L_2 \sin \alpha \right\} - \mu V \left[\frac{1}{h_T} + \frac{1}{h_B} \right] L_3 = 0 \quad (14)$$

Because the assumption was made that W is equal on all sides [see Fig. 14(e)], this parameter drops out of Eq. (14). The driving force is multiplied by a factor of two to account for the two liquid films on each side of the vapor slug. The homogeneous flow regime experiments yielded an average velocity for the slug of 61 mm/s. For this average velocity, and with the values of radii of curvature and height as determined in Figs. 14(a) and 14(b), a top shear layer height of $14.6 \pm 3 \mu m$ is obtained from the model.

The phenomenological model presented in this section is based on some key assumptions, namely that (a) the liquid layer height is uniform, (b) the vapor pressure within the slug is uniform, and (c) the shape of the bubble is assumed to be of the form shown in Fig. 14(e). The model can be used to predict the slug velocity, given all other measured parameters. Hence, the pumping effect of the passive geometry can be quantified by the model. The limitation is that several critical liquid layer thickness measurements are required for the model to be able to predict this velocity. Future work to measure the top shear layer thickness and validate the calculated value is warranted. Additionally, experiments that visualize the cross-sectional shape of the bubble are needed. Such measurements would require simultaneous visualization from two different directions.

4. CONCLUSIONS

The impact of two types of surface asymmetry on the two-phase flow during boiling has been presented. The first type of asymmetry was created by locating cavities preferentially on one face of a periodically structured surface (or ratchets). The second type of asymmetry was created by a difference in the face angles of the ratchets. Directional growth of bubbles released in concert from a ratcheted surface, and self-propulsion of vapor slugs in an open channel using asymmetry in surface structure is demonstrated.

Asymmetry caused by preferential location of cavities was studied in a pool-boiling facility. Directional growth of the bubble perpendicular to the ratchet face was observed over a range of heat flux and subcooling conditions for the dielectric fluid FC-72. Bubble growth was characterized by a rapid inertia-controlled regime exhibiting a linear growth rate with time, followed by a slower heat transfer controlled regime that exhibited a power-law relation with an exponent of 0.24.

Asymmetry due to ratchet angle was studied using an open-channel setup. Three distinct regimes of self-propulsion were observed for the range of studied experimental conditions: bubble regime, churn flow regime, and the intermittent slug regime. Bubble and slug velocities as high as 95 mm/s were observed in the range of heat flux and subcooling studied. A model based on asymmetry in pressure gradient as the driving force and viscous shear as the retarding force is proposed to explain the self-propulsion. Such self-propulsion can be of great importance in developing pumpless thermal management loops with high heat removal capacity for applications such as electronics cooling and spacecraft thermal management, especially in microgravity environments.

ACKNOWLEDGMENTS

Financial assistance for the project was provided by NSF under Grant Nos. 0854503 and 0854132 and by NASA under Grant Nos. NNX09AJ98G and NNX09AL63G. Contributions of Eric Truong and Florian Kapsenberg to the experimental parts of the project are acknowledged. Discussions with Dr. Heiner Linke, Professor of Nanophysics at Lund University, are gratefully acknowledged.

REFERENCES

- Cole, R. and Shulman, H.L., Bubble Growth Rates at High Jakob Numbers, *Int. J. Heat Mass Transf.*, vol. 9, pp. 1377–1390, 1966.
- Demiray, F. and Kim, J., Microscale Heat Transfer Measurements during Pool Boiling of FC-72: Effect of Subcooling, *Int. J. Heat Mass Transf.*, vol. 47, pp. 3257–3268, 2004.
- Hutter, C., Kenning, D., Sefi, K., Karayiannis, T., Lin, H., Cummins, G., and Walton, A., Experimental Pool Boiling Investigations of FC-72 on Silicon with Artificial Cavities and Integrated Temperature Microsensors, Exp. Therm. Fluid Sci., vol. 34, pp. 422–433, 2010.
- Jun, T.K. and Kim, C.-J., Valveless Pumping Using Traversing Vapor Bubbles in Microchannels, *J. Appl. Phys.*, vol. **83**, pp. 5658–5664, 1998.
- Kapsenberg, F., Thiagarajan, N., Narayanan, V., and Bhavnani, S.H., Lateral Motion of Bubbles from Surfaces with Mini Ratchet Topography Modifications during Pool Boiling-Experiments and Preliminary Model, Proc. of the 13th Intersociety Conf. on Thermal and Thermomechanical Phenomena in Electronic Systems (ITherm-2012), pp. 165–175, San Diego, CA, May 30–June 1, 2012.
- Lee, H.C., Oh, B.D., Bae, S.W., and Kim, M.H., Single Bubble Growth in Saturated Pool Boiling on a Constant Wall Temperature Surface, *Int. J. Multiphase Flow*, vol. **29**, pp. 1857–1874, 2003.
- Linke, H., Alemian, B.J., Melling, L.D., Taormina, M.J., Francis, M., Dow-Hygelund, C.C., Narayanan, V., Taylor, R.P., and Stout, A., Self-Propelled Leidenfrost Droplets, *Phys. Rev. Lett.*, vol. 96, p. 154502, 2006.
- Mikic, B. and Rohsenow, W., Bubble Growth Rates in Non-Uniform Temperature Field, *Prog. Heat Mass Transf.*, vol. **2**, pp. 283–293, 1969.

- Mikic, B., Rohsenow, W., and Griffith, P., On Bubble Growth Rates, *Int. J. Heat Mass Transf.*, vol. 13, pp. 657–666, 1970.
- Ok, J., Lopez-Ona, E., Nikitopoulos, D., Wong, H., and Park, S., Propulsion of Droplets on Micro- and Sub-Micron Ratchet Surfaces in the Leidenfrost Temperature Regime, *Microfluid. Nanofluid.*, vol. 10, no. 5, pp. 1045–1054, 2011.
- Plesset, M. and Zwick S.A., The Growth of Vapor Bubbles in Superheated Liquids, *J. Appl. Phys.*, vol. **25**, pp. 493–500, 1954.
- Ramaswamy, C., Joshi, Y., Nakayama, W., and Johnson, W., High-Speed Visualization of Boiling from an Enhanced Structure, *Int. J. Heat Mass Transf.*, vol. **45**, pp. 4761–4771, 2002.
- Rayleigh, L., On the Pressure Developed in a Liquid during the Collapse of a Spherical Cavity, *London, Edinburgh, Dublin Philos. Mag. J. Sci.*, vol. **34**, pp. 94–98, 1917.
- Scriven, L., On the Dynamics of Phase Growth, Chem. Eng. Sci., vol. 10, pp. 1–13, 1959.
- Thiagarajan, N., Kapsenberg, F., Narayanan, V., Bhavnani, S.H., and Ellis, C.D., Development of a Heat Sink with Periodic Asymmetric Structures Using Grayscale Lithography and Deep Reactive Ion Etching, *Electron Device Lett.*, vol. **33**, pp. 1054–1056, 2012.
- Thiagarajan, N., Kapsenberg, F., Narayanan, V., Bhavnani, S.H., and Ellis, C.D., Phase-Change Actuated Pumping on an Asymmetric Augmented Surface: Design and Feasibility, *ASME InterPACK 2011 Conf.*, Portland, OR, Paper No. IPACK2011-52054, July 6–8, 2011.
- van Stralen, S., Sohal, M., Cole, R., and Sluyter, W., Bubble Growth Rates in Pure and Binary Systems: Combined Effect of Relaxation and Evaporation Microlayers, *Int. J. Heat Mass Transf.*, vol. **18**, pp. 453–467, 1975.
- Yuan, H. and Prosperetti, A., The Pumping Effect of Growing and Collapsing Bubbles in a Tube, J. Micromech. Microeng., vol. 9, p. 402, 1999.
- Zuber, N., The Dynamics of Vapor Bubbles in Non-Uniform Temperature Field, *Int. J. Heat Mass Transf.*, vol. **2**, pp. 83–98, 1961.